JOURNAL OF AIRCRAFT
Vol. 43, No. 4, July–August 2006

Drag Reductions Possible with Aircraft Employing Outboard Horizontal Stabilizers

J. A. C. Kentfield*
University of Calgary, Calgary, Alberta T2N 1N4, Canada

The potential of using outboard horizontal stabilizers (OHS) to reduce aircraft drag and, hence, improve fuel economy was investigated both experimentally and theoretically. The feasibility of OHS configurations on the basis of the structural stress levels expected was also studied. The overall findings of the survey showed that from simple, low-Reynolds-number wind-tunnel tests at a wing-chord-based Reynolds number of approximately 6×10^4, and also from theoretical analyses for a higher Reynolds number of 9×10^6, lift/drag value increases in the region of 30 to 50% for wing and tail surfaces can be expected relative to corresponding values for conventional aircraft. The analytical stress-level work showed that contrary to what, on a first-thought basis, might be expected, there were no major stress problems. Flight tests employing radio-controlled, powered, model aircraft, that is, unmanned aerial vehicles, showed that aircraft of the OHS type were easily controlled in flight and were stable. An examination was made of additional areas that may contribute yet further to the development of the OHS concept.

Nomenclature

a	=	downwind displacement of c.g. from mean aerodynamic chord (MAC)/4
AR	=	aspect ratio
b	=	wing semispan
C_L	=	lift coefficient
C_M	=	pitching moment coefficient
c	=	chord, at MAC station
D	=	drag
e	=	Oswald efficiency factor
L	=	aerodynamic lift
L'	=	distance from $c_w/4$ to $c_{\mathrm{TH}}/4$
n	=	multiple of c_w, origin at outboard face of tail boom
S	=	projected or planform area of aerodynamic surface
U	=	flight velocity
W	=	weight
w	=	downwash velocity, positive downward
x	=	distance aft from wing leading edge
Y	=	y/b
y	=	spanwise displacement from center of wing
α	=	wing angle of incidence, deg
$\bar{\alpha}$	=	average angle of incidence with wing washout or twist
ε	=	downwash angle, positive downward
Θ	=	static margin, distance from c.g. to neutral point)/c_w

Subscripts

a.c.	=	aerodynamic center
c.p.	=	center of pressure (at MAC station)
$c/4$	=	quarter-chord location (at MAC station)
L	=	lateral inflow, ε as positive when acting toward aircraft vertical plane of symmetry
TH	=	tail horizontal
TV	=	tail vertical
U	=	upwash, operates on ε to change sign to positive upward
W	=	wing

Presented as Paper 2005-0811 at the AIAA 43rd Aerospace Sciences Meeting and Exhibition, Reno, NV, 10–13 January 2005; received 15 March 2005; revision received 19 July 2005; accepted for publication 20 July 2005.

*Professor Emeritus, Department of Mechanical and Manufacturing Engineering. Senior Member AIAA.

Introduction

AN outboard horizontal-stabilizer (OHS) aircraft configuration is one in which both of the horizontal-stabilizer surfaces are carried, outboard of a wing tip, on booms projecting downwind from the wing tips. This, therefore, results in each horizontal-stabilizer surface becoming immersed in the downstream directed upwash flowfield generated by the wing tip upstream. This implies that if each horizontal-stabilizer surface is employed not only for aircraft pitch control purposes, as is normally the case for conventional aircraft, but also as a lift-generating surface, the lift vector will be inclined forward in the flight direction, thereby helping to cancel the drag of the tail. For it to be feasible to employ the horizontal-stabilizer surfaces as lift generators, it will normally be necessary to move the center of gravity of an OHS aircraft substantially farther aft than the 25 to 30% of the wing mean aerodynamic chord (MAC) commonly employed with conventional aircraft, for which the horizontal stabilizer usually generates zero lift or a small negative lift.

The vertical tail surfaces of an OHS configuration will usually be mounted at, or close to, the downwind end of the booms, supporting the horizontal stabilizers. If the vertical surfaces are mounted such as to project above the booms, these surfaces will experience an inwash flow component also resulting from the wing-tip generated flowfield. This will result, for vertical surfaces aligned with the flight direction, in transverse lift forces acting primarily toward the vehicle central plane of symmetry but with components inclined in the flight direction, thereby helping to cancel the drag of the vertical tail surfaces. Alternatively, if the vertical tail surfaces are changed to project downward below the booms, a similar overall affect can be obtained, but in this case the flowfield is such that the transverse lift force acts outward, away from the vehicle central plane of symmetry, but still gives rise to force components inclined in the flight direction thereby also helping to cancel vertical surface drag. Clearly, from the viewpoint of maximizing ground clearance, etc., it is desirable to mount the vertical surfaces above, rather than below, the booms. It would appear to be particularly undesirable for a single vertical tail surface to project both above and below a tail boom because this will cause the upper portion of the inner face of such a vertical surface to be subjected to suction while, simultaneously, the lower portion of the inner face is subjected to an overpressure.

It will be shown, later, that the flow inclinations toward the tail surfaces resulting from the wing-tip flowfields are very important contributors helping to cancel tail-induced, and skin-friction, drags. In fact, it will be shown that for many flight conditions the flow inclinations to the tail surfaces result in complete cancellation of tail drags and the generation of small net thrusts from the tail surfaces of OHS configurations.

It will also be shown later, both experimentally and theoretically, that the OHS concept is applicable to both nonswept, or straight-winged, aircraft configurations with fairly modest subsonic cruise Mach numbers and also swept-wing and tail designs suitable for high subsonic cruise Mach numbers. For a swept-wing OHS configuration, the wings will be preferentially swept forward, relative to the fuselage, to preserve, for a significantly elastic structure, structural stability. This situation is the opposite to that prevailing for conventionally designed high subsonic Mach number aircraft. However, in both cases, for OHS and conventionally designed aircraft, the wings are swept rearward relative to the pitch-control surfaces that, for OHS designs, are attached via booms to the wing tips. For a classical, conventional design, due to a combined bending and torsional loading, a transient upload to the wing tends to produce a torque that decreases the angle of incidence at the wing tip. With an OHS configuration, a transient wing upload produces a torque that reduces the wing angle of attack near the central fuselage, thereby tending to tilt the fuselage slightly nose down. In both cases, the opposite influences are expected with transient downloads or load reductions. The leading edges of the horizontal and vertical tail surfaces of high subsonic Mach numbers OHS aircraft should be swept rearward as with conventional designs. If the wing structure is exceedingly stiff, for example, as might be the case for a very low wing aspect ratio, an OHS configuration with rear-swept wings may be acceptable. This certainly has the advantage, relative to forward sweep, of reducing the boom length required.

The application of the OHS concept to high subsonic Mach numbers raises the specter of the use of so-called supercritical wing sections to delay, as much as possible, the onset of supersonic flow over wing suction surfaces. Supercritical wings are noted for relatively large negative pitching moment coefficients in the region of -0.15 or thereabouts. An analysis is presented that shows that high subsonic Mach number OHS configurations, and other OHS aircraft, can be designed to take into account negative pitching moments of the required magnitude. This avoids restricting OHS aircraft to symmetric wing cross sections or prohibiting the use of high-lift devices or, worse yet, demanding the use of less effective reflex, or negative camber, wing airfoil sections to produce nose-up pitching moments.

Figure 1 shows a small jet-propelled transport with a 20-deg forward wing-sweep angle. The OHS concept, which has been investigated for a number of years, is not the only form of aircraft configuration with outboard mounted tail surfaces. An overview of past work on this topic is presented in the Historical Background section of Ref. 1.

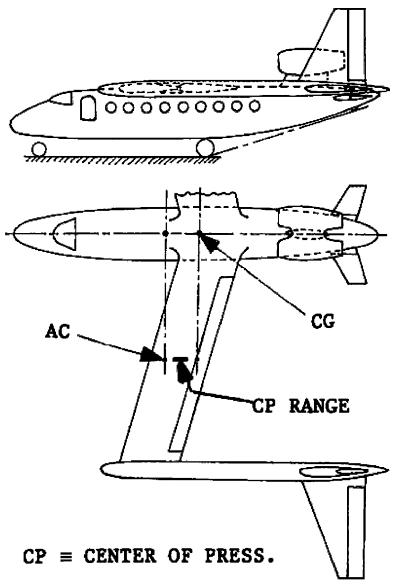

Fig. 1 Twin-jet, high subsonic Mach number passenger aircraft with super-critical wing; small surfaces at end of fuselage are pitch dampers set to zero angle of incidence relative to local flow.

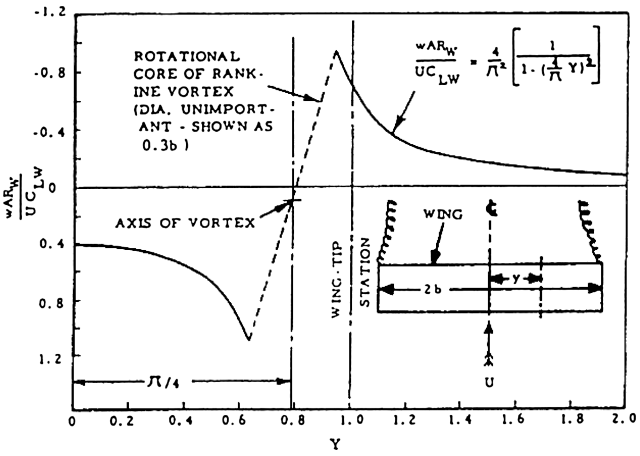

Fig. 2 Flowfield far downstream of elliptically loaded wing.

Experimental Performance

The primary measurements made to establish the inherent performances of OHS configurations involved wind-tunnel testing and also a backup process involving flow visualization tests employing colored-dye tracer flows in a water tunnel in which a small-scale, nonswept wing OHS model was suspended. An initial notional expectation of the flow upwash magnitude outboard, and well downstream, of the tips of an elliptically loaded wing was obtained from the work of Glauert.[2] According to an approximate formulation,[3] vortex rollup is complete at a distance of approximately $8b$ downstream of the wing, resulting in the wake downwash and upwash profiles as presented in Fig. 2. Note from Fig. 2 that the upwash profiles outboard of the wing tips can be represented by an average upwash angle of 18.3 deg (C_{LW}/AR_W), for horizontal stabilizer surfaces, each of a span equal to 40% of the wing semispan (that is, $0.4b$), a value typical of many conventional aircraft. As a first approximation, this upwash magnitude was assumed to prevail closer to the wing tip than at a distance of $8b$ downstream of the wing. Strictly speaking, for a simple elliptically loaded wing, the wing shown as a simple rectangle in Fig. 2 should, of course, be shown as a surface with an elliptical planform. The upwash profile shown in Fig. 2 suggests the use of tapered horizontal stabilizers to better utilize the stronger upwash flow close to the wing tips. Further thought suggests the desirability of achieving the horizontal-stabilizer taper by sweeping back the leading edges. This will tend to have an effect similar to building wash-in to the horizontal stabilizers to assist in ameliorating, and spreading, the upwash peaks close to the wing tips.[4]

Wind-Tunnel Tests (Nonswept Wing)

Wind-tunnel tests were carried out to compare, experimentally, the performances of comparable OHS and conventional nonswept wing aircraft configurations. The tests were restricted to relatively low Reynolds numbers, in the region of 6×10^4, based on the mainplane chord, due to the dimensions and flow speed of the available open-jet wind tunnel that had a jet width of 1.372 m (54 in.) and a jet depth of 0.762 m (30 in.). The span, over the tips of the horizontal stabilizers of the OHS configuration was 0.795 m (31.3 in.). The aspect ratio of the mainplane was 6.19, including the booms supporting each half of the horizontal stabilizer, and was 5.92 for the wing alone with the booms removed. The planform area of both halves of the horizontal stabilizer was 40% of the mainplane planform area. The span of each half of the horizontal stabilizer was 40% of the wing semispan. The corresponding conventional configuration employed the same mainplane and horizontal stabilizer surfaces as the OHS model. This commonality ensured that any differences in test results between the two configurations would not be a consequence of manufacturing errors in the fabrication of either the mainplane, which was of NACA 0018 section, or the horizontal stabilizers that had a thickness/chord ratio of approximately 12%. Figure 3 is a photograph of the OHS version of the wind-tunnel model, and Fig. 4

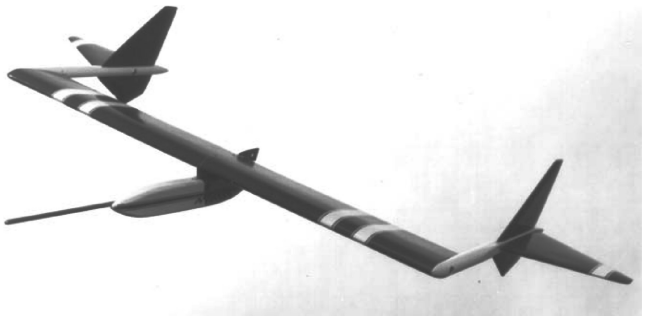

Fig. 3 Photograph of OHS version of wind-tunnel model aircraft.

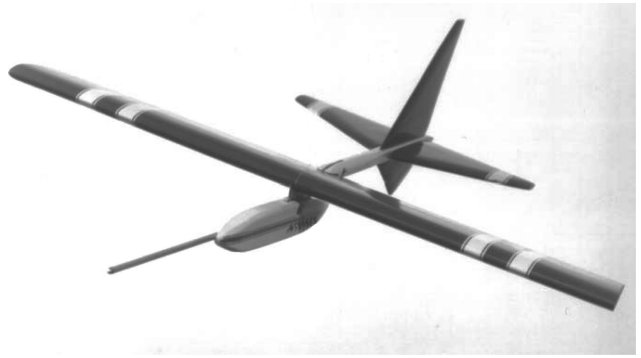

Fig. 4 Photograph of conventional version of wind-tunnel model aircraft.

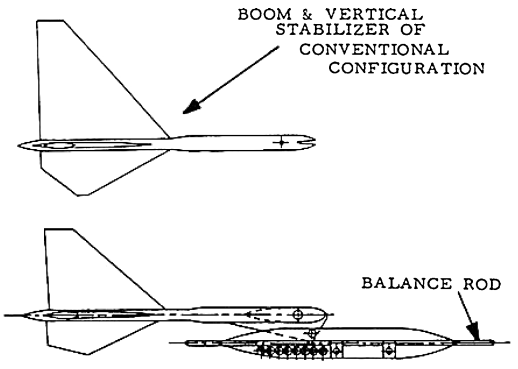

Fig. 5 Diagram, to scale, of interchangeable wind-tunnel models of Figs. 3 and 4.

shows the corresponding conventional version. Figure 5 is a reproduction of part of the fabricational drawing from which the model components were constructed, showing more details of the models than can be deduced from Figs. 3 and 4.

The test data recorded included the model lift and drag and the flow speed of the tests, in addition to geometric settings of the model such as wing and horizontal-stabilizer incidence angles. For each test, the model was mounted inverted in the wind tunnel on a lift and drag balance, being supported by a hinge pin from one of the holes, apparent in Fig. 5, in the fuselage component. The hole selected for a test was that located vertically above, in the inverted model, the desired location of the c.g. The model was balanced in the fore and aft direction by sliding forward or rearward the metal rod (Figs. 3 and 4) attached to the fuselage component. A pointer moving over a scale revealed any deviation from the horizontal setting during the operation of the wind tunnel. This would then be corrected by adjusting the angle of incidence of the horizontal stabilizers to bring the fuselage back to the horizontal position. The wind-tunnel blockage due to the model was less than 3.5% of the tunnel flow cross-sectional area, for the most extreme operating condition.

Table 1 *L/D* ratios for equal lift for nonswept wings[a]

Configuration	Corrected wind-tunnel results, $Re = 6 \times 10^4$	Predicted results, $Re = 6 \times 10^4$
OHS	9.122	8.661
Conventional	6.962	7.006
Σ drag (OHS)/Σ drag (conventional)	0.763	0.809

[a]Based on optimum L/D for conventional configuration.

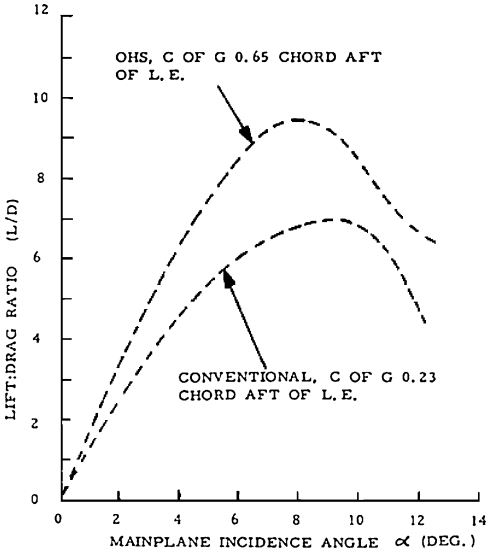

Fig. 6 Performance comparison, in terms of *L/D* ratio vs mainplane incidence angle, of wind-tunnel performances of OHS and conventional configurations; uncorrected wind-tunnel data.

A summary of the results obtained from the wind-tunnel tests were presented in the form of lift/drag (L/D) curves vs wing angle of incidence α for the OHS configuration and the corresponding conventional arrangement. Figure 6 shows a comparison of the two curves, the upper one for the OHS configuration with the c.g. located at 65% of the mainplane chord aft of the mainplane leading edge and the lower one for the conventional configuration with the c.g. at 23% of the mainplane chord aft of the leading edge. Both of these c.g. positions were in the middle of the range explored for each case. As can be seen very clearly from Fig. 6, the maximum L/D of the OHS configuration was approximately 35% greater than that of the conventional version of the model. The drag forces were approximately equal for both versions of the wind-tunnel model, but the lift was significantly greater for the OHS version. The difference between the L/D ratios of the two versions of the model is greater than would be expected if the parasitic drags due to powerplants had been included and if the model had been provided with a large cross-sectional fuselage representative of a realistic transport. An attempt was also made to establish an optimum setting of the vertical stabilizers of the OHS version of the model. It was only found to be possible to achieve a very small performance improvement by this means.

For equal lift situations, a comparison was made of the performances of the OHS and conventional version of the model based on the wind-tunnel test data corrected using the methods recommended by Piercy,[5] to take into account the factors influencing the accuracy of these data. The predicted results also took into account a procedure described by Hoerner[6] for estimating the drag losses expected from the intersection of the tail-support boom with the wing suction surface of the conventional version of the model. The results of the performance comparison are presented in Table 1. Note that the experimental result for the OHS configuration may possibly be superior to the predicted value because flow inclined to the vertical stabilizers may generate a lift force, skewed to the line of flight, sufficient to offset the drag of these surfaces. When this

assumption is applied to the prediction procedure, the OHS L/D increases from 8.661 to 9.193, and the predicted drag ratio is reduced from 0.809 to 0.762. The modified predicted values are then in almost perfect agreement with the experimental results. Further details of the wind-tunnel testing carried out on the nonswept wing OHS and conventional configurations are available elsewhere.[7]

Water-Tunnel Tests

Flow visualization tests were carried out in a water tunnel in which a small model of the nonswept OHS configuration was installed. The purpose of these tests was to obtain complementary information to that obtained from wind-tunnel testing concerning local flow in the region of a mainplane tip and the adjacent horizontal and vertical stabilizer surfaces. The tunnel was of the vertical downflow type and followed a design originated by H. Werle of ONERA (see Ref. 8).

The Reynolds number of the tests was unavoidably low due to the need to prevent turbulent mixing of the thin flow-visualization streams (condensed milk colored with food dye) in the main flow and around the model. As a consequence of this restriction, the Reynolds number of the bulk flow in the transparent working section of the tunnel was approximately 7×10^3, whereas that based on the mainplane chord of the model was only about 5×10^2. Despite these restrictions, the tests did reveal upwash occurring outboard of the tip of the lifting mainplane, this flow then being deflected, rather as might be expected, by the projecting adjacent horizontal-stabilizer surface. A strong inward flow deflection around the vertical stabilizers was also apparent. These tests served, therefore, to provide visual confirmation of the expected flow mechanism. They also served to provide partial justification for the modification to the OHS performance prediction procedure mentioned earlier with respect to Table 1.

Wind-Tunnel Tests (Swept Wing)

The wind-tunnel tests with swept wings as would likely be required for high subsonic Mach numbers were also carried out using the open-jet facility that was used for earlier tests with nonswept wings. Accordingly, the same NACA-0018 wing as for the earlier work was modified by cutting the original solid-wood wing to provide, after reassembly, a nontapered wing with 25-deg forward sweep as shown in Fig. 7. The aspect ratio of the modified wing was 4.98, or with the inclusion of the wing extensions due to the tail support booms, 5.18. The thickness of the modified NACA-0018 section measured in the freestream direction was 16.3%. The planform areas of the original nontapered, nonswept, and the modified swept wing were, of course, equal. The selection of a 25-deg sweep angle was typical of the one-quarter chord aft-swept angles of several high subsonic Mach number aircraft, for example, the Boeing 737, McDonnell Douglas DC-8 and DC-9, and several Dassault executive jets.

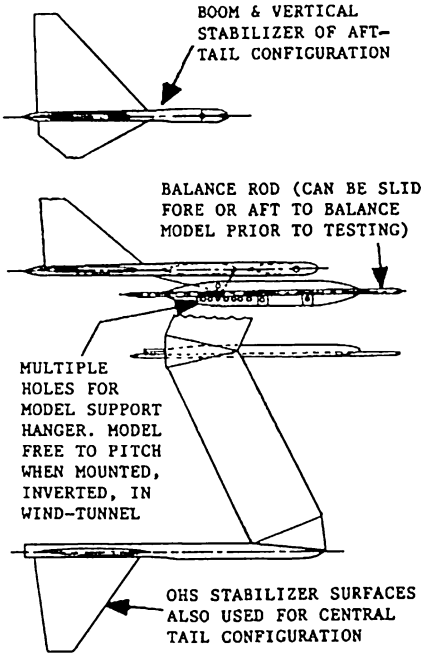

Fig. 7 Wind-tunnel model for low-speed tests of OHS configuration with 25 deg of forward wing sweep and for testing a swept-forward configuration with central tail.

The wind-tunnel tests of the forward-swept wing with the conventional, centrally located, aft-tail assembly were undertaken merely for the purpose of comparison with the corresponding results for the forward-swept-wing OHS configuration. A heavily forward-swept wing used in conjunction with a conventional central tail would normally be expected to be structurally unstable, due to a coupled bending and torsional effect, in a full-scale unit with an elastic wing structure. However, no such structural instability was noted with the relatively rigid solid-wood wing of the wind-tunnel model.

A typical wing-chord-based Reynolds number of approximately 6.5×10^4 was representative of the low-speed swept-wing wind-tunnel tests. The same tail surfaces were used for the swept-wing tests that had been used earlier for the nonswept wing work. The leading edges of the horizontal and vertical stabilizers were already sufficiently swept back to be representative of high subsonic Mach number flight, and, hence, no modifications were required, although the ventral fins of the outboard vertical surfaces (Fig. 5) were omitted, as is apparent in Fig. 7.

Relative to the earlier tests with a nonswept wing, the length of the OHS booms were increased, and that of the central boom decreased, to maintain for the forward-swept wing tests the same tail moment-arm lengths that prevailed for the earlier tests. The model was tested, as for the nonswept tests, inverted in the tunnel. The model was also supported on a pivoted mount attached to the lift balance such that it was free to rotate in pitch. As was the case for the the preceding tests, the model was balanced about the selected pivot location on the model by means of adjustment, fore or aft, of the balance rod (Fig. 7) to set the fuselage of the model horizontal for static conditions. The horizontal setting of the fuselage of the model was maintained, during each test, by adjustment of the incidence angle of the all flying horizontal stabilizers. Before each test the wing incidence angle, relative to the fuselage, was set to the desired wing incidence angle for that particular test.

Comparative results for the forward-swept OHS and central-tail configurations are shown in Fig. 8 in terms of configuration L/D vs incidence angle α. The pivot location at which the OHS model was supported was 0.65 of the wing MAC aft of the wing leading edge, and the support location for the centrally tailed configuration was 0.28 of the MAC aft of the wing leading edge. Note from Fig. 8, that the OHS configuration produced results only from approximately 17 to 20% better, in terms of L/D, than those obtained with the central conventional tail.

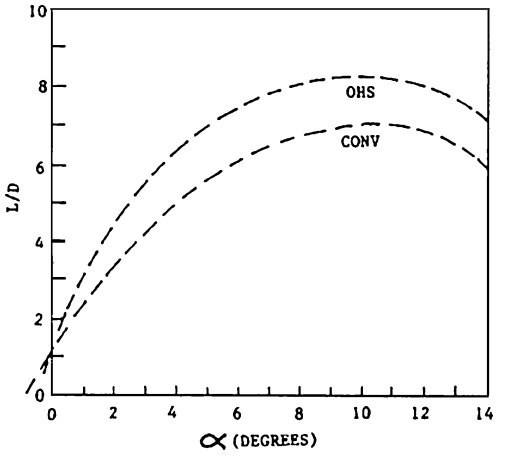

Fig. 8 Comparison of experimental data showing superior *L/D* values of OHS configuration.

The comparatively small benefit accruing from the OHS configuration relative to the performance of the swept wing with the centrally located tail compared with the relative benefit of the OHS configuration with nonswept wings noted in earlier work[7] suggested the possibility that flow could, perhaps, be separating from the inner portion of the wing suction surface. Such flow separation would be likely to hurt the performance of the OHS configuration, but for the configuration with the centrally located tail assembly the horizontal stabilizers may well help to generate lift in a compensatory manner. Accordingly, a simple flow visualization test served to confirm a significant area of flow separation at an incidence angle of 10 deg as shown in Fig. 9. It was felt that this problem was due, primarily, to the swept nature of the wing and was exacerbated by the low Reynolds number of the wind-tunnel tests.

Accordingly, to introduce a measure of washout toward the center of the solid-wood wing, the wing was cut, as shown in Fig. 10, to introduce discontinuous washout steps by means of which the wing was effectively twisted by 3 deg. This cured, effectively, the wing flow separation problem, and the modified wing configuration shown in Fig. 10 was employed for the remainder of the tests with the forward-swept wing.

The results of tests with 3 deg of wing washout from the boom toward the central fuselage are presented in Fig. 11. The effective

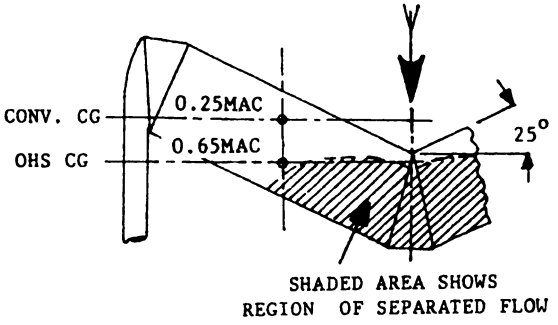

Fig. 9 Region of flow separation of model forward-swept wind-tunnel wing at 10-deg angle of incidence.

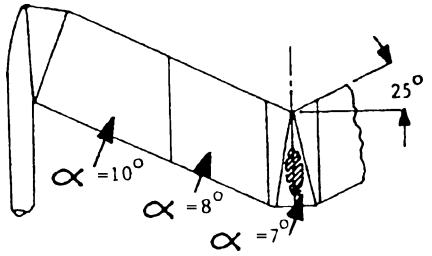

Fig. 10 Reduced regions of flow separation with simulated 3-deg washout from wing tip toward aircraft centerline.

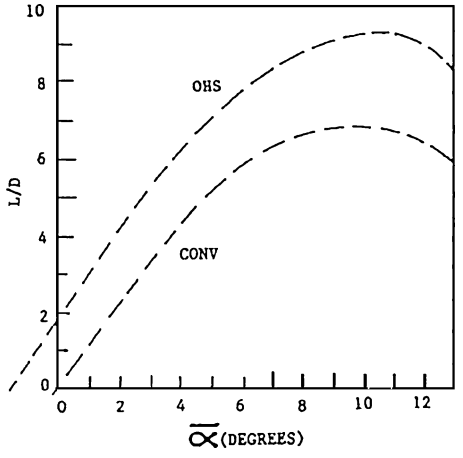

Fig. 11 Comparison of experimental data with significantly superior *L/D* values of OHS configuration with wing twist.

angle of incidence $\bar{\alpha}$ deg at 0 deg corresponds to a positive angle of incidence of 1 deg for the outer wing panels with a negative angle of incidence of 1 deg for the adjacent inner panels and a negative incidence angle of 2 deg for the small innermost central portion of the wing. It is probably this situation that leads to an L/D ratio of 2 at a zero value of $\bar{\alpha}$. The peak L/D value was found to be approximately 9.2 at a value of $\bar{\alpha} = 10.5$-deg. This value is slightly less than the peak value of 9.5 realized from earlier tests with a nonswept wing[7] but is significantly greater than the value of 8.2 at $\alpha = 10$ deg obtained with the nontwisted forward-swept wing. The ratio of the peak values of L/D obtained with the twisted swept-forward wing was approximately 0.74, the same as the value found earlier[7] with the nonswept nontwisted wing, showing that the peak L/D values with a central-tail configuration were only about three-quarters of the corresponding values obtainable with an OHS configuration for both nonswept and swept-forward wings when the latter are provided with suitable washout.

Wind-Tunnel Test: Summary

A high subsonic Mach number aircraft is not likely to employ a wing of symmetric section as used for the wind-tunnel tests but, instead, a so-called supercritical wing of asymmetric section that is usually characterized by having a significant negative pitching moment coefficient (of about –0.15). Thus, the experimentally obtained results for the symmetric section swept-forward wing were later modified, by theoretical means, to accommodate this. In terms of the work reported here, the major difference between a conventional symmetric wing section and a supercritical section was expected to be the negative pitching moment of the latter.

For all of the wind-tunnel tests of model aircraft, all of which were free to move in the pitch direction, with conventional central tails and also with OHS configurations of both nonswept and forward-swept wings, no instability in the pitch mode was observed. This suggests, but does not prove, due to the models all having a small degree of pendulum-action induced stability, that the static margins of the models were probably adequate. However, it remained to prove by analytical means whether or not adequate static margins prevailed.

More details of the wind-tunnel tests of the model aircraft with the forward-swept wing are available.[9] Very recent work using particle image velocimetry equipment serves to confirm the flow picture around the tail surfaces established by more commonly used flow-visualization techniques.

Performance Predictions

To make meaningful predictions of the performance of OHS aircraft it is necessary to revise the notional relationship describing flow outboard of the tips of a wing presented in Fig. 2. That relationship applies to the expected flow outboard of the tips of an elliptically loaded wing far downstream of the wing, in the region of four wingspans or so downstream. The requirement was to establish the flowfield prevailing downwind and outboard of the wing tips as functions of both wing lift coefficient C_{LW} and wing aspect ratio AR_W.

It was proposed to establish the required data experimentally by wind-tunnel tests conducted on a nonswept wing of invariant cross-sectional dimensions but of variable aspect ratio. However, a potential problem relating to this approach was that the facilities available restricted the tests to turbulent flow with a wing-chord-based Reynolds number of only 6×10^4.

Although the separated vortexlike flow in the region of a wing tip was not expected to be a strong function of wing Reynolds number, it was thought desirable to verify this assumption by comparing results obtained in the author's facility with data obtained at significantly higher wing Reynolds numbers. Such a comparison is presented in Fig. 12 which shows upwash flow angles ε_u vs the displacement outboard of a tail-support boom of thickness 0.1 c_w, measured as multiples n of the chord of the rectangular planform wing. Each solid line represents results obtained in the University of Calgary facilities, with the OHS stabilizer surfaces removed, for aspect ratios covering the range $4 \leq \mathrm{AR}_W \leq 11$. There is no apparent

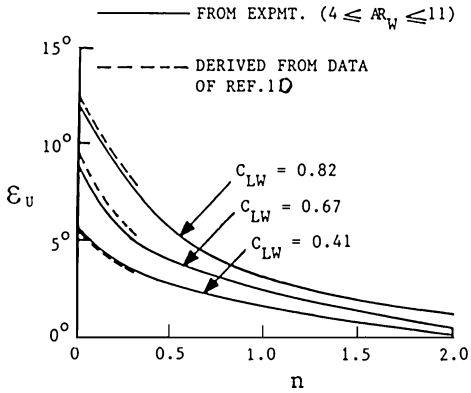

Fig. 12 Comparison of upwash flow measurements (no tail surfaces).

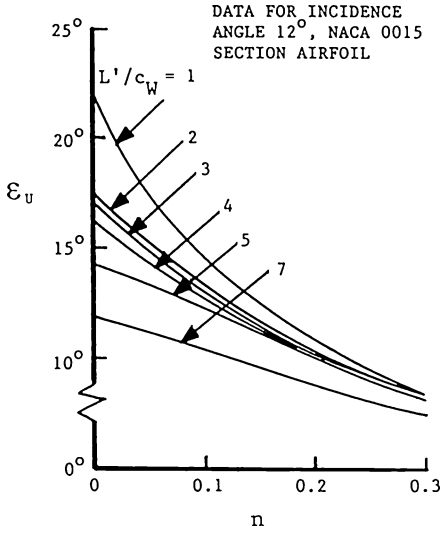

Fig. 13 Variation of upwash flow with downwind displacement L'/c_w.

influence of aspect ratio. The dotted lines were derived from the data of McAlister and Takahashi[10] for a wing-chord-based Reynolds number of 1.5×10^6. Although the McAlister and Takahashi data extend only to an n value of 0.3, it can be seen that there is reasonable agreement between the solid and dotted curves, tending to confirm that near-wing-tip flows are not strong functions of wing-chord-based Reynolds number.

The results by McAlister and Takahashi[10] can also be used to establish the variation of upwash flow angle ε_u with tail surfaces absent as a function of the tail downwind displacement parameter L'/c_w. These results are shown, in Fig. 13 for an angle of incidence of 12 deg for McAlister and Takahashi's NACA 0015 aspect ratio 6.6 wing sections at a Reynolds number of 1.5×10^6. The range of L'/c_w values of practical interest for the present study is from 2 to 4. Within that range it appears that, to a first-order approximation, the upwash flow angle as a function of n is independent of L'/c_w.

Horizontal-Stabilizer Upwash Flowfield

Tests similar to those reported in the preceding section with no horizontal tail surfaces attached to the tail support boom were carried out, with the vertical stabilizer installed, at the design location at the downwind end of the tail-support boom. Variable wing aspect ratio, over the range $4 \leq AR_W \leq 11$, was simulated by projecting an available NACA 0018 section airfoil of uniform chord through a splitter plate installed in the wind tunnel to represent a plane of symmetry between the portion of the OHS configuration modeled and that which was omitted. The wing tip projecting into the test area was provided with a tail-support boom and also, as stated earlier, a vertical stabilizer surface.

These results obtained in this manner are represented by the solid lines in Fig. 14. The dotted curves show the output of an analytical equation modeling the potential flow of a wing-tip vortex far downstream of an aircraft as presented in Fig. 2. The equation is rearranged slightly to give

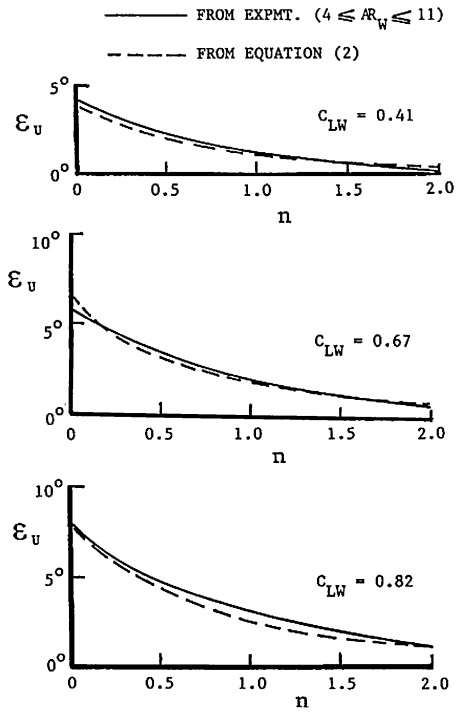

Fig. 14 Upwash flow angle over horizontal stabilizer.

$$\frac{w}{U} = \frac{C_{LW}}{AR_W}\frac{4}{\pi^2}\left\{\frac{1}{1-[(4/\pi)Y]^2}\right\} \tag{1}$$

and then modified empirically to describe the angle ε_u of the upwash flow in the region $2 \leq L'/c_w \leq 4$, with account taken of the observed independence of ε_u on AR_w, the replacement of Y in terms of n, and the outward displacement from the wing tip of the horizontal stabilizer by the thickness of the boom, namely, $0.1\,c_w$ These modifications led to the final result when ε_u is expressed in degrees and assigned as positive for an upwash flow,

$$\varepsilon_U = C_{LW}\left\{\frac{3.871}{[(4/\pi)(1.0333+n/3)]^2-1}\right\}\left(1.7667-\frac{n}{3}\right) \tag{2}$$

Vertical-Stabilizer Lateral Flowfield

Wind-tunnel tests were also carried out to establish the lateral, or inwash flowfields acting on the vertical-stabilizers. For this work the vertical-stabilizer surface of the half-model OHS configuration was removed, and the horizontal-stabilizer surface was installed at a realistic decalage angle of −6 deg relative to the wing.

Similar to the upwash flow situation, it was found that the inwash flow was effectively independent of the mainplane aspect ratio AR_W. The results obtained are shown as solid lines in Fig. 15. The dotted curves shown the results obtained from use of Eq. (2) multiplied by a factor of 1.6, thus,

$$\varepsilon_L = 1.6\varepsilon_u \tag{3}$$

where ε_u was evaluated from Eq. (2). It is clear that the fit to the experimental results is not quite as good as for the upwash case, although it appears to be adequate for preliminary design purposes. The factor of 1.6 between the inwash and upwash flow angles is, apparently, due to an inflow induction occurring on top of, and also downwind of, the mainplane. This effect is essentially complementary to the wing-tip generated vortex action.

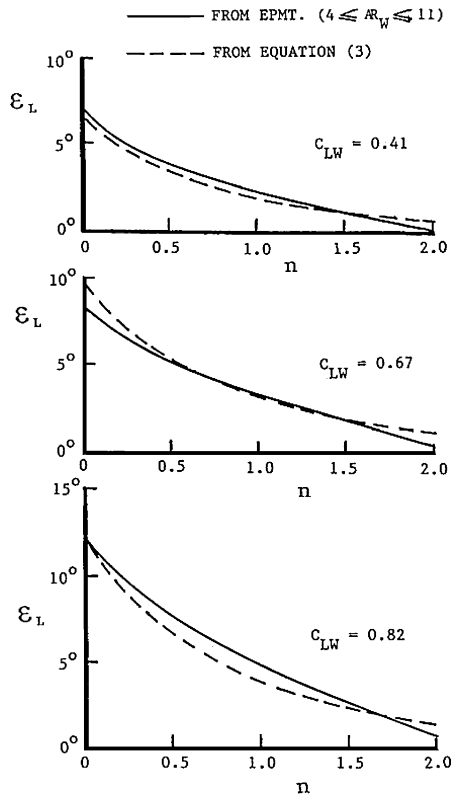

Fig. 15 Inwash, or lateral, flow angle over vertical stabilizer.

Pitch Stability

In a previous study of a relatively conservatively designed nonswept wing OHS vehicle and a comparable conventional aircraft, each of aspect ratio six, the influences of three values of the pitch static margin θ of 0.17, 0.23, and 0.32 were compared.[11] It was decided to maintain a constant θ value of 0.23 for all cases. However, because θ is defined as the distance between the neutral point and the c.g. divided by the wing chord, for aircraft of prescribed wing area, an increase in aspect ratio implies a reduction of absolute static stability in pitch.

In a previous study of OHS and conventional aircraft of aspect ratio six[11] the Oswald efficiency factor of the mainplane was assigned the conservative value of 0.8. Here the values of Oswald efficiency were evaluated from an empirical relationship, attributed to Cavallo,[12] applicable to straight wings in the form

$$e = 1.78(1 - 0.045AR^{0.68}) - 0.64 \tag{4}$$

Equation (4) purports to be used on data derived from real aircraft and to include the adverse influence on wing performance of the junction between the mainplane and the fuselage. Equation (4) was also applied to the horizontal stabilizers of the conventional aircraft studied. Because the interaction of flaps on aircraft performance and the elevator settings required to maintain level flight over a range of wing lift coefficients have been investigated in detail in a previous study,[11] these topics are not considered here. Hence, attention is confined to establishing the comparative influences of mainplane aspect ratio on the performances of OHS configurations and otherwise comparable conventional aircraft over a range of lift coefficients, in straight, level flight.

Configurations Investigated (nonswept Wings)

The configurations investigated in the study include only the aerodynamic surfaces (no fuselages or tail booms) of OHS and otherwise comparable conventional configurations. For all of the turbulent flow studies, the wing section selected was a NACA 2412, which has a pitching moment coefficient of -0.05, and that for the horizontal and vertical stabilizers was a NACA 0012. For all of the OHS configurations the c.g. location was assumed to be 65% of the wing chord aft of the wing leading edge and for the conventional configurations 25% aft of the wing leading edge. The latter condition results in a constant negative tail-plane lift coefficient independent of C_{LW} and weakly dependent on AR_W. For all turbulent flow studies, it was also assumed that for all aerodynamic surfaces the two-dimensional drag coefficient C_{D0} had a value of 0.008 to allow for the presence of hinge lines where movable control surfaces joined the fixed portions of the aerodynamic surfaces. For simulated laminar-flow operation, C_{D0} was relaxed to a value of 0.005, where it is assumed that good sealing and fairing was provided between the fixed and movable portions of the aerodynamic surfaces of the laminar-flow wing and tails.

The horizontal-tail lift coefficient C_{LTH} necessary to sustain level flight was evaluated by moments for both conventional and OHS vehicles, leading to the result

$$C_{LTH} = \frac{(a/c_w)C_{LW} + C_{M(c/4)w} + (c_{TH}S_{TH}/c_wS_w)C_{M(c/4)TH}}{(S_{TH}/S_W)(L'/c_w - a/c_w)} \tag{5}$$

where $C_{M(c/4)\,TH}$ is zero for the cases considered here for zero elevator trim because symmetric sections were selected for the horizontal-stabilizers of both the OHS and conventional aircraft. When C_{LTH} derived from Eq. (5) was not compatible with prevailing conditions, the elevators were assumed to be positioned to adjust C_{LTH} to the required value deduced from Eq. (5).

For the effective upwash and inflow angles impinging on the tails of OHS configurations, area-weighted analyses were performed on the half-tapered tail surfaces incorporating values of ε_u and ε_L obtained from Eqs. (2) and (3), respectively, yielding ε_u and ε_L in terms of C_{LW} for prescribed tail-surface aspect ratios. The latter were based on twice the span of each tail half-surface due to a combination of the massive end plate effect of the vertical tail surfaces plus the upwash distribution over each horizontal tail surface. The downwash due to the wings at the tails of conventional aircraft was established using a procedure describe by McCormick.[13]

On the basis of guidance derived from Figs. 14 and 15, note that the influence of the wing-tip flow prevails for a maximum spanwise direction and also vertically for a distance approximately equal to twice the chord of the wing. It was found subsequently for OHS configurations that the best performances were obtained when each horizontal stabilizer projected two wing chords outboard of the tail-support boom. However, it was also found that the best vertical-stabilizer performances were obtained with slightly shorter, and, therefore, lower aspect ratio, vertical stabilizers thereby giving a better tradeoff between induced drag and ε_L. The geometric details of the substantially optimized OHS configurations obtained in this manner for AR_W values between 6 and 15 are shown in Fig. 16 for a static margin of 0.23. For all of the conventional arrangements, also with a static margin θ of 0.23, the horizontal stabilizer area divided by the wing area, S_{TH}/S_W, was 0.2 with a horizontal stabilizer aspect

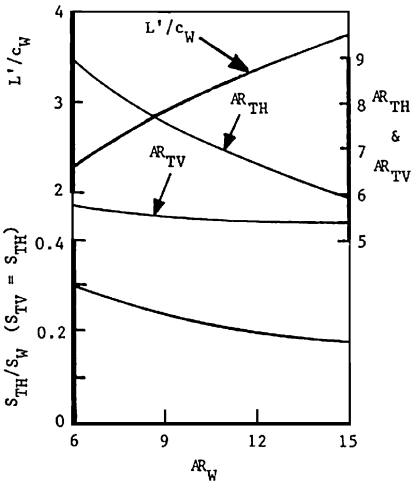

Fig. 16 Geometric parameters of optimized OHS configurations.

ratio A_{TH} of 4. The vertical stabilizer area was 75% of that of the horizontal stabilizer. For the OHS designs the area of the vertical stabilizers was made equal to that of the corresponding horizontal tails. For the OHS configurations the values of C_{LTH} were within the range from 0.45 to 0.62 of the corresponding C_{LW} values. This, therefore, allowed a sufficient margin for the horizontal stabilizers to also function as pitch-control surfaces.

Predicted Performances (Nonswept Wings)

Figure 17 shows the predicted performance L/D vs C_{LW}, for the OHS-type arrangements of aerodynamic surfaces. The locus of the peaks shows that the peak C_{LW} values equivalent to wing plus tail loads range from approximately 0.64 with $AR_W = 6$ to nearly 0.71 when $AR_W = 15$. The applicable wing-chord-based Reynolds number is 9×10^6. The maximum L/D value with $AR_W = 15$ is 37.

Corresponding data for the comparable conventional configurations, for nonlifting horizontal tails, are presented in Fig. 18 for the same C_{LW} range. Here the peak values of C_{LW} range from 0.45 when $AR_W = 6$ to nearly 0.6 when $AR_W = 15$. The peak L/D value with $AR_W = 15$ is just under 26. Figure 19 shows a comparison of the OHS and conventional data for equal lifts in terms of the ratio of OHS drag divided by that of corresponding conventional configurations vs C_{LW} with parameters of AR_W. Note from Fig. 19 that the relative advantage of the OHS arrangement tends to diminish as AR_W is increased and to increase as C_{LW} increases. Figure 20 shows another form of performance comparison based on the loci of the peaks in Figs. 17 and 18. Here it can be seen that the L/D ratio of the conventional configuration is essentially 69% of that of the OHS configuration of equal AR_W over the range $6 \leq AR_w \leq 15$.

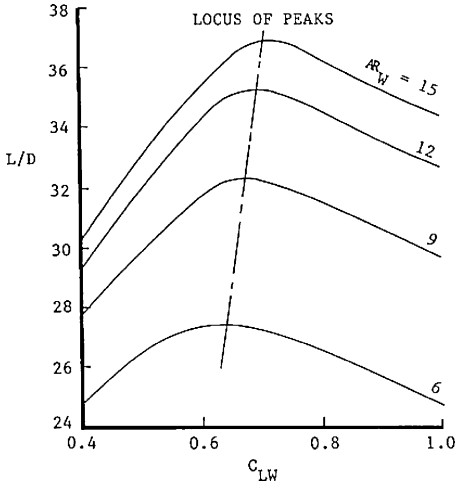

Fig. 17 *L/D* of aerodynamic surfaces vs C_{LW} of optimized OHS configurations.

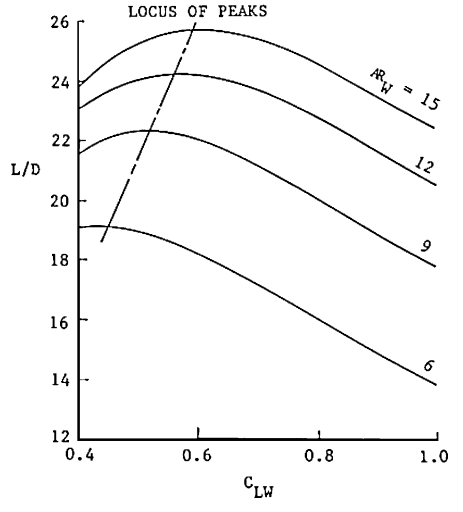

Fig. 18 *L/D* of aerodynamic surfaces vs C_{LW} of comparative conventional configurations.

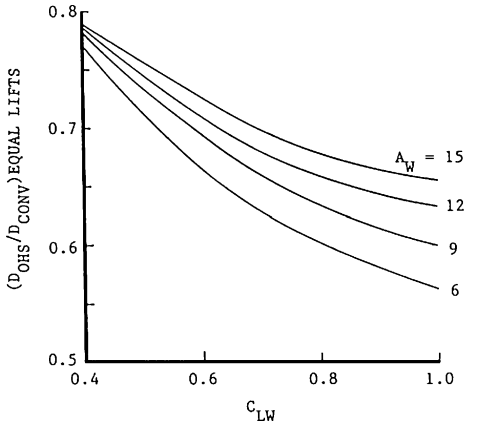

Fig. 19 Ratio of drags of OHS aerodynamic surfaces to those of conventional configurations vs C_{LW} for turbulent flow conditions.

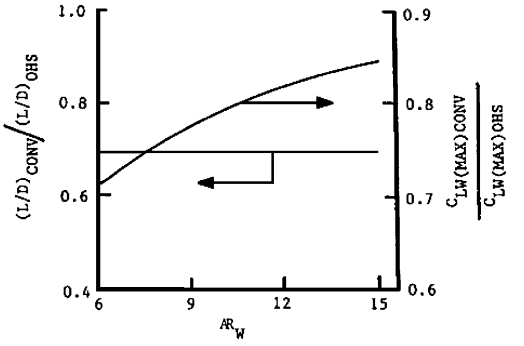

Fig. 20 Comparison of *L/D* ratios and C_{LW} ratios based on loci of peaks presented in Figs. 17 and 18.

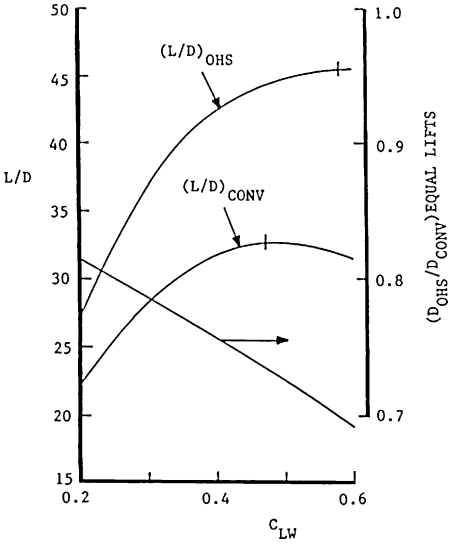

Fig. 21 Ratio of drag of OHS aerodynamic surfaces to that of corresponding conventional configuration, laminar-flow conditions, $AR_W = 15$.

It seems likely that very high aspect ratio configurations would incorporate laminar-flow surfaces. Accordingly, Fig. 21 shows a performance comparison, for an AR_W value of 15, between OHS and conventionally configured arrangements. The airfoils selected were NACA 65_2–415 for wings, which has a pitching moment coefficient of -0.05, and NACA 64_2–015 for tail surfaces, which is

a symmetric section and, therefore, has a zero pitching moment coefficient. The C_{LW} range covered is reduced relative to the turbulent flow comparisons of Figs. 17–20 due to the need to remain within the drag bucket regions of the airfoils. The optimum C_{LW} value for the conventional configuration is approximately 0.47, whereas it is 0.58 for the OHS configuration. Comparison of Fig. 21 with Fig. 19 shows that the decay of the ratio of the OHS drag to that of the conventional configuration is more rapid for the laminar case than that applicable to turbulent flow. Under laminar flow conditions, for $AR_W = 15$, the peak L/D value for the OHS configuration was 45 and for the conventional arrangement it was slightly greater than 32.

Predicted Performances (Swept Wings)

The performance prediction procedures used with swept-forward wing are, essentially, the same as those used with nonswept wing systems. One difference in detail involves the location of the c.g. With nonswept, uniform chord wings the c.g. selected can be expressed simply in terms of the distance $(a + 0.25)$ aft of the wing leading edge. With swept wings of uniform chord $(a + 0.25)$ is specified as the distance aft of the leading edge at the MAC station. The tail moment arm, L'/c_w, is measured, as for nonswept wings, with the exception that the point of origin on the wing is at the quarter-chord location at the MAC station.

The evaluation of the required value of C_{LTH} is obtained from Eq. (5) as for the nonswept wing cases. For wing sweep angles of 30 deg or less, Cavallo's equation (4) remains unaltered for the estimation of the Oswald efficiency factor e included in the expression $C_L^2/\pi e AR_W$ for evaluating the wing induced drag coefficient. The use of McCormick's procedure[13] remains the same as for the nonswept wing cases for evaluating the static margin θ, noting, of course, that for OHS configurations the horizontal-stabilizer surfaces remain in an upwash flowfield rather than in the downwash flow usually associated with conventional configurations with a central tail located in the wake generated by the wing.

Two performance predictions each were made for forward-swept-wing OHS configurations and for (hypothetical) conventional designs with a central tail also used in conjunction with a forward-swept wing. One OHS and one conventional design were analyzed for cases with symmetrical cross-sectional wings with zero wing-generated pitching moments, as were one OHS and one conventional design employing an asymmetric cross-sectional wing producing a pitching moment coefficient of -0.15, representative of a so-called supercritical swept wing likely to be used on high subsonic Mach number aircraft. For each analysis, $S_{TH}/S_W = 0.3$.

For the symmetric wing-section OHS case Eq. (5) was used for evaluating L'/c_w when $C_{LTH} = 0.5C_{LW}$, a very reasonable choice enabling the horizontal stabilizers to function jointly as lifting and pitch-control surfaces. This yielded a value of L'/c_W of 3.067 with the c.g. at 65% of the wing chord aft of the wing leading edge corresponding to $a/c_w = 0.4$. This resulted in the chain-dashed line in Fig. 22 presenting C_{LTH} vs C_{LW} and also the upper solid curve in

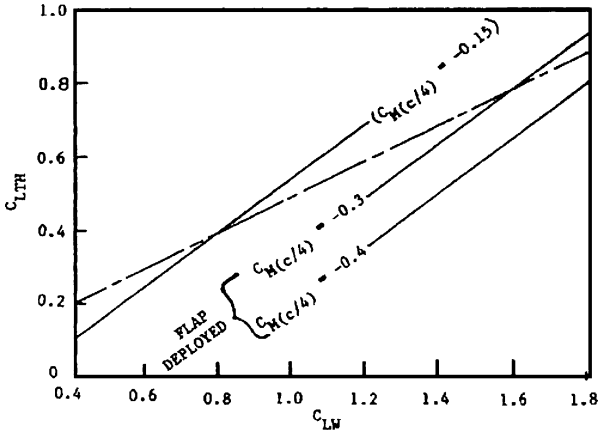

Fig. 22 Horizontal-stabilizer lift coefficient C_{LTH} vs wing lift coefficient C_{LW} for symmetric wing sections and corresponding data for asymmetric wings, from theoretical analysis, $AR_W = 6$, swept-wing case.

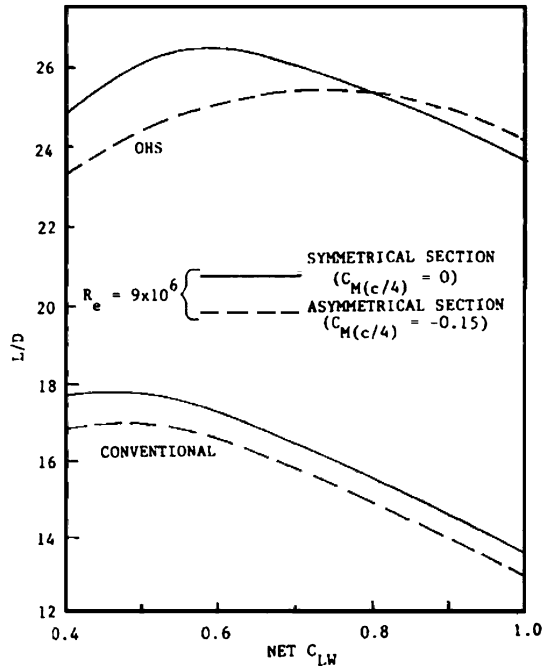

Fig. 23 Theoretically derived *L/D* ratios for OHS and conventional, swept-wing configurations with symmetric and asymmetric airfoil sections: wing aspect ratio = 6, effective horizontal-stabilizer aspect ratio = 8, wing-chord-based Reynolds number $\cong 9 \times 10^6$.

Fig. 23. Both Figs. 22 and 23 apply to a wing aspect ratio AR_W of 6. The lower solid curve in Fig. 23 applies to a conventional (central tail) arrangement with a symmetric section wing with the c.g. located at the quarter-chord point of the MAC station. The horizontal tail of this configuration is, therefore, nominally unloaded.

The performance prediction with an airfoil-generated negative pitching moment coefficient of $(-)$ 0.15 leads to matching the value of $C_{LTH} = 0.5C_{LW}$ at a selected value of C_{LW} such that C_{LTH} overshoots $0.5C_{LW}$ by an amount approximately equal to the extent that C_{LTH} undershoots $0.5C_{LW}$ at the top and bottom, respectively, of the operational range of C_{LW} from approximately $C_{LW} = 1.1$ to (approximately) $C_{LW} = 0.4$. This consideration lead to choosing the condition that $C_{LTH} = 0.5C_{LW}$ when $C_{LW} = 0.8$. Applying this particular condition to Eq. (5) lead to the result that $L'/c_w = 2.967$ when the c.g. is located as far as possible toward the trailing edge of the airfoil, consistent with obtaining a satisfactory static margin of $\theta \approx 0.2$. This in turn, indicates that the c.g. should be no farther aft than 0.8 of the wing chord from the wing leading edge, giving a value of $a/c_w = 0.55$.

This situation leads to the evaluation of the upper dashed curve of Fig. 23 for the OHS configuration. The lower dashed curve of Fig. 23 is the result of applying the moment coefficient –0.15 to the central tail arrangement, thereby giving rise to a tail lift coefficient of -0.1685 when the c.g. is located at the quarter-chord location of the MAC station with

$$L'/c_w = 2.967, \qquad S_{TH}/S_W = 0.3$$

More details of the performance prediction procedures reviewed here are available elsewhere.[9,14] In Ref. 9 swept-wing configurations are covered, and in Ref. 14 the application of performance prediction procedures for nonswept wing aircraft are covered. In both cases, OHS and conventional arrangements are compared.

Structural Considerations

A major consideration relating to the practicality of the OHS concept relates to the stress levels likely to occur relative to those in otherwise comparable conventional aircraft. The expression otherwise comparable was taken to imply essentially similar vehicles of the conventional and OHS types, the major difference between them

being the better fuel utilization and, therefore, the greater range, of the OHS aircraft. Clearly, other forms of comparison could be involved, for example, similar missions of equal range and with equal payloads undertaken at equal flight speeds or, possibly, missions of equal range and with equal payloads but undertaken at unequal flight speeds and/or at different altitudes or combinations of these sets of conditions.

A detailed comparative design study was performed on the basis of the easiest of the foregoing criteria, namely, aircraft benefiting from a range increase due to substituting a relatively low-drag OHS configuration for a conventional design. The comparison was based on a small commuter-type vehicle. The essential findings were that, in the most general sense, and contrary to what might be expected intuitively, an OHS configuration did not result in stress level problems.[15]

A study was also made to establish the relative merits of OHS and conventional aircraft designs for prescribed missions when the criterion of similarity involved equal takeoff thrust-to-weight ratios for the OHS and corresponding comparative conventional design. Further details are available elsewhere.[16]

Flight Tests of OHS Models

Numerous flight tests were made, over a period of years, on large-scale, radio-controlled, models of OHS aircraft. In most cases the flight characteristics of the models were studied by observation. In general, the pilots of the models, mostly recruited from the local model aircraft community, reported favorably on the flying characteristics of these aircraft. In two cases the flights were recorded, extensively, on video, and in one additional case instrumented tests were conducted, at a graduate student level, of an electronic autonomous control system developed especially for OHS-type aircraft. The whole topic is discussed in much more detail elsewhere.[1]

Development Potential

Reasons for OHS Concept Success

A question that may be asked is why the relatively simple conceptual idea of placing the horizontal stabilizer surfaces outboard and aft of the wing tips results in the promise of drag reductions compared with conventional configurations. The main reasons for this were touched upon in the Introduction. The factors in favor of a drag reduction include, for a prescribed gross lift 1) smaller mainplane, 2) increased vehicle overall aspect ratio,[17] 3) tail lift, and 4) reduction of tail drag due to the forward inclination of the aerodynamic lift forces generated by these surfaces. This effect also extends to the vertical stabilizers. Hence, total cancellation of both the induced and skin-friction drag is a possibility for most flight conditions of practical interest with the production of a small net thrust. These matters are discussed in more detail elsewhere.[1]

Minimization of Fuselage/Wing Interference Drag

With conventional aircraft, a simplistic rule of thumb implies that aircraft drag has very approximately two main components of equal magnitude, namely, fuselage drag and the drag of the aerodynamic surfaces, that is, wing and tail surfaces. This suggests that it is very desirable to minimize fuselage drag and wing/fuselage interference drag. With an OHS configuration the fuselage is essentially of the pod type and, therefore, tends to be shorter for a given cross-sectional area than a conventional fuselage.

It has already been shown, on the basis of preliminary experimental work,[18] to be possible to benefit, in terms of a reduction of fuselage drag, by invoking and utilizing a wing-generated pressure field with high-wing OHS vehicles. The inherent problem with this is that the wing needs to be mounted far back along the fuselage. This implies a balancing problem in that most of the payload will be carried ahead of the nominal c.g.

OHS Counterpart to Formation Flight

At the commencement of the OHS work a rectangular mainplane planform was selected primarily for structural reasons. Subsequent work[19] has shown, on a theoretical basis, that this planform appears to be optimum for formation flying because this strengthens the upwash flow-field benefit for a correctly positioned following aircraft. For the OHS case the following aircraft is represented by the tail surfaces.

The benefit to the following aircraft appears to be that achievable with a single OHS aircraft in terms of the drag savings possible. About 20% has been demonstrated by means of formation flying tests by the downwind vehicle of a pair of conventional aircraft.[20]

Summary

The work described covers the main operating characteristics of the OHS configuration. Results of low-speed wind-tunnel tests of nonswept- and swept-wing OHS configurations are summarized. Performance predictions based on a wing-chord-based Reynolds number of about 9×10^6, a value representative of relatively small full-scale aircraft, showed that on the basis of comparative predicted performances of the aerodynamic surfaces only, that is, main wing and tail surfaces, a comparison of the L/D ratios for OHS and alternative conventional configurations showed that the OHS values are typically 40–50% greater with an estimated accuracy of $\pm 10\%$ of these values.

A review of the comparative stress levels of OHS and conventional aircraft suggests that the OHS concept does not introduce major stress problems, although there are differences between the stress generating mechanisms of the two aircraft types.

Flight tests of powered, radio-controlled, OHS models revealed flight characteristics similar to, but not identical with, those of conventional aircraft. This feature resulted in generally favorable comments from the pilots of the model aircraft once they had gained familiarity with the models. Finally, an account was presented describing the multiple factors that, collectively, resulted in the considerable promise in terms of significantly improved performance of OHS configurations as measured in terms of L/D ratio.

On the basis of the results reported, and the work undertaken to date, it was concluded that the OHS concept has been validated as an effective drag saving system with much potential for many practical applications.

Acknowledgments

The author is indebted to undergraduate students, too numerous to identify individually, who, over a period of years, constructed flying, radio-controlled, model outboard horizontal-stabilizer (OHS) aircraft which, for the most part, were the vehicles from which significant OHS flight experience was gained by the University of Calgary. Two of these students who subsequently continued with graduate studies involving OHS configurations were Jason Mukherjee, who obtained his Ph.D. at the University of Calgary, and Sarah Saleh, who became a graduate student in aeronautical engineering at the Massachusetts Institute of Technology. The Department of Mechanical and Manufacturing Engineering at the University of Calgary is also grateful to members of the model aircraft community who served as pilots for the OHS model aircraft flight-test program.

References

[1]Kentfield, J. A. C., "Drag Reduction and Improved Fuel Economy of Aircraft Employing Outboard Horizontal Stabilizers," *Journal of Aircraft*, Vol. 43, No. 4, 2006, pp. 964–974.

[2]Glauert, H., *Elements of Aerofoil and Airscrew Theory*, 2nd ed., Cambridge Univ. Press, Cambridge, England, U.K., 1948, Chap. 2, pp. 156–170.

[3]Hoerner, S. F., and Borst, H., *Fluid Dynamic Lift,* 1st ed., Hoerner Fluid Dynamics, Albuquerque, NM, 1975, Chap. 3, pp. 1, 2.

[4]Kentfield, J. A. C., "Aircraft Configurations with Outboard Horizontal Stabilizers," *Journal of Aircraft*, Vol. 28, No. 10, 1991, pp. 670–672.

[5]Piercy, N. A. V., *Aerodynamics,* 2nd ed., English Univ. Press, London, 1950, pp. 335–344.

[6]Hoerner, S. F., *Fluid Dynamic Drag,* 2nd ed., Hoerner Fluid Dynamics, Albuquerque, NM, 1965, Chap. 8, pp. 15, 16.

[7]Kentfield, J. A. C., "Case for Aircraft with Outboard Horizontal Stabilizers," *Journal of Aircraft*, Vol. 32, No. 2, 1995, pp. 398–403.

[8]Tycholis, T., "Calibration and Operation of the O.N.E.R.A. Water Tunnel," Rept. 132, Dept. of Mechanical Engineering, Univ. of Calgary, Calgary, AB, Canada, Oct. 1978.

[9]Kentfield, J. A. C., and Spragins, A., "Swept-Wing Outboard-Horizontal-Stabilizer Aircraft Configuration," *Journal of Aircraft*, Vol. 41, No. 1, 2004, pp. 144–150.

[10]McAlister, K. W., and Takahashi, R. K., "NACA 0015 Wing Pressure and Trailing Vortex Measurements," NASA TP-3151, 1991; also U.S. Army Aviation Systems Command, TR 91-A-003, 1991.

[11]Kentfield, J. A. C., "Upwash Flowfields at the Tails of Aircraft with Outboard Horizontal Stabilizers," AIAA Paper 98-0757, Jan. 1998.

[12]Cavallo, B., "Subsonic Drag Estimation Methods," U.S. Naval Air Development Center Rept. NADC-AW-6604, 1966.

[13]McCormick, B. W., *Aerodynamics Aeronautics and Flight Mechanics*, 2nd ed., Wiley, New York, Chap. 12, 1995, pp. 473–482.

[14]Kentfield, J. A. C., "Influence of Aspect Ratio on the Performance of Outboard Horizontal-Stabilizer Aircraft," *Journal of Aircraft*, Vol. 37, No. 1, 2000, pp. 62–67.

[15]Kentfield, J. A. C., "Structural Loading of Outboard Horizontal-Stabilizer Aircraft Relative to Comparable Conventional Designs," *Journal of Aircraft*, Vol. 38, No. 1, 2001, pp. 174–180.

[16]Kentfield, J. A. C., "The Fuel Economy Potential of Outboard-Horizontal-Stabilizer Aircraft," AIAA Paper 2004-1238, Jan. 2004.

[17]Munk, M., "The Minimum Drag of Airfoils," NACA Rept. 121, 1921.

[18]Kentfield, J. A. C., and Jones, H. L., "Fuselage–Wing Interference Drag of Aircraft with Relatively Short, Pod-Type Fuselages," AIAA Paper 2002-0708, Jan. 2002.

[19]Iylesias, S., and Mason, W. H., "Optimum Spanloads in Formation Flight," AIAA Paper 2002-0258, Jan. 2002.

[20]Ianotta, B., "Vortex Draws Research Forward," *Aerospace America*, Vol. 40, No. 3, 2002, pp. 26–30.